On the Seasonality of Arctic Haze

Zhaoyi Shen*

Program in Atmospheric and Oceanic Sciences, Princeton University, Princeton, New Jersey.

Yi Ming, Larry W. Horowitz, V. Ramaswamy and Meiyun Lin

NOAA/Geophysical Fluid Dynamics Laboratory, Princeton, New Jersey.

Corresponding author address: Zhaoyi Shen, NOAA Geophysical Fluid Dynamics Laboratory, 201 Forrestal Rd., Princeton, NJ 08540.

E-mail: zs@princeton.edu

ABSTRACT

Arctic haze has a distinct seasonality with peak concentrations in winter but pristine conditions in summer. It is demonstrated that the Geophysical Fluid Dynamics Laboratory (GFDL) atmospheric general circulation model AM3 can reproduce the observed seasonality of Arctic black carbon (BC), an important component of Arctic haze. We use the model to study how large-scale circulation and removal drive the seasonal cycle of Arctic BC. It is found that despite large seasonal shifts in the general circulation pattern, the transport of BC into the Arctic varies little throughout the year. The seasonal cycle of Arctic BC is attributed mostly to variations in the controlling factors of wet removal, namely the hydrophilic fraction of BC and wet deposition efficiency of hydrophilic BC. Specifically, a confluence of low hydrophilic fraction and weak wet deposition, owing to slower aging process and less efficient mixed-phase cloud scavenging, respectively, is responsible for the wintertime peak of BC. The transition to low BC in summer is the consequence of a gradual increase in the wet deposition efficiency, while the increase of BC in late fall can be explained by a sharp decrease in the hydrophilic fraction. The results presented here suggest that future changes in the aging and wet deposition processes can potentially alter the concentrations of Arctic aerosols and their climate effects.

1. Introduction

The accumulation of visibility-reducing aerosols in the Arctic during late winter and early spring (known as Arctic haze) was first discovered in the 1950s (Mitchell 1957). The haze has its root cause in the long-range transport of air pollution originating from the mid-latitude industrial regions (Barrie 1986), and can have an influence on Arctic climate (Law and Stohl 2007). The haze is a mixture of both light-scattering and light-absorbing aerosols. The aerosols pose strong radiative perturbations by scattering and/or absorbing solar radiation, by interacting with clouds, and by reducing the surface albedo when deposited onto snow and ice (Quinn et al. 2007). The surface temperature in the Arctic increased more than the global average since the late 20th century, coinciding with a rapid decline of sea ice (Bindoff et al. 2013). Besides greenhouse gases, decreased (increased) scattering (absorbing) aerosols were postulated to have contributed to this amplified Arctic climate change (Shindell and Faluvegi 2009).

Sulfate and black carbon (BC) are the dominant scattering and absorbing aerosols in the Arctic, respectively (Law and Stohl 2007). Distinct seasonal cycles of Arctic sulfate and BC concentrations are present in measurements. Surface observations at Alert and Barrow show that BC concentrations tend to peak during late winter and early spring before starting to decline in April, and reach a minimum during summer (Sharma et al. 2006). Aircraft measurements of sulfate reveal similar seasonal variations, with aerosol layers at higher altitudes persisting into May (Scheuer 2003).

Different hypotheses have been posited to explain the seasonal cycle of Arctic haze. Previous studies have shown that European emissions dominate Arctic aerosols, with smaller contributions from East Asia and North America (e.g., Stohl 2006; Shindell et al. 2008). A dynamically oriented view holds that during the haze season (winter and spring), meridional transport from mid-latitude

source regions to the Arctic is stronger due to vigorous large-scale circulation. The presence of Siberian high pressure helps steer polluted European air into the Arctic by transient and stationary eddies (Barrie 1986; Iversen and Joranger 1985). The diabatic cooling of air traveling over ice and snow also facilitates transport to the Arctic lower troposphere. In contrast, pollution is diabatically transported to higher altitudes and diluted in summer (Klonecki et al. 2003).

A competing theory is that Arctic haze occurs in winter owing to slower removal. As a major sink term for aerosols, wet scavenging by precipitation (rain and snow) is modulated heavily by cloud microphysics. Aerosols are not effectively removed by ice clouds since soluble aerosols such as sulfate are generally poor ice nuclei (IN). BC particles become effective IN only when the temperature is below $\sim$240 K (Friedman et al. 2011). In mixed-phase clouds, the Bergeron process (i.e. evaporation of liquid droplets in the presence of ice crystals) releases aerosols contained in cloud droplets back into air (Cozic et al. 2008), so the wet scavenging in mixed-phase clouds is much less efficient than in liquid clouds (Liu et al. 2011; Browse et al. 2012). The low efficiency of ice cloud and mixed-phase cloud scavenging favors accumulation of aerosols at cold temperatures. Dry deposition also has seasonal variations and is weaker in winter when the stable boundary layer inhibits turbulent mixing (Quinn et al. 2007). It, however, accounts for only a small portion of the total removal and affects mainly the surface concentrations of Arctic haze (Liu et al. 2011). Another key factor unique to BC is the aging process, which refers to the transformation from hydrophobic to hydrophilic aerosols due to coating by soluble species (Petters et al. 2006). Only aged BC particles can act as cloud condensation nuclei (CCN) and be removed by in-cloud scavenging. As a result, the aging rate has a large effect on global BC concentrations and distributions. Experimental studies have found that condensation of gaseous sulfuric acid (H_2SO_4) is an effective aging mechanism for BC particles (Zhang et al. 2008); reduced concentrations of H_2SO_4

due to slower oxidation of SO_2 by the hydroxyl radical (OH) in winter results in a lower aging rate and thus weaker wet deposition (Liu et al. 2011).

It is important to note that the aforementioned mechanisms (namely large-scale circulation, cloud microphysics and aging) are not mutually exclusive; they could all act to induce seasonality. Yet, the relative importance of these mechanisms in shaping the pronounced seasonal cycle of Arctic haze remains unclear. While it is hard to separate these factors cleanly using observations alone, we approach the issue here using a comprehensive global model. In this study we apply an atmospheric general circulation model (AGCM) to analyze the factors controlling the seasonal cycle of Arctic haze with a focus on BC, an important constituent of Arctic haze with a potentially important influence on Arctic climate.

2. Model Description

This study uses the Geophysical Fluid Dynamics Laboratory (GFDL) AM3 AGCM (Donner et al. 2011) with a cubed-sphere grid resolution of $\sim$100 km and 48 hybrid vertical levels from the surface to $\sim$1 Pa. We conduct a six-year hindcast simulation (2008-2013), following one year of spin-up. The emission inventories reflect 2008-2013 conditions. Anthropogenic emissions of aerosol and ozone precursors with seasonal variations are based on Hemispheric Transport of Air Pollution (HTAP) v2 - a mosaic of regional and global emission inventories for the years 2008 and 2010 (Janssens-Maenhout et al. 2015), and are held constant after 2010. Daily-resolving biomass burning emissions for 2008-2013 are adopted from the Fire Inventory from National Center for Atmospheric Research (NCAR) (Wiedinmyer et al. 2011) and emitted in the model surface layer. The model is forced with observed sea surface temperatures and sea ice, and horizontal winds are nudged to the reanalyses from the National Centers for Environmental Prediction (NCEP) Global Forecasting System at approximately $1.4^\circ \times 1.4^\circ$ horizontal resolution using a pressure-dependent

nudging technique (Lin et al. 2012). The latter makes it possible to compare model simulations with observations for specific flight campaigns.

The treatment of BC in AM3 used in this study differs from that described by Donner et al. (2011), and has been discussed extensively by Liu et al. (2011) and Fan et al. (2012); here we summarize briefly the key features. AM3 includes two types of BC: hydrophobic (BCpo) and hydrophilic (BCpi). 80% (40%) of BC emitted from anthropogenic (biomass burning) sources is assumed to be hydrophobic. The hydrophobic BC is then converted to the hydrophilic form at a variable aging rate (Liu et al. 2011), which depends on condensation of sulfuric acid (the rate of which is assumed to be proportional to OH concentrations) and other processes such as coagulation (represented by adding a small constant term to the aging rate coefficient, see Section 6 for more discussion). Only hydrophilic BC can be removed by in-cloud scavenging, which is parameterized using a first-order rate coefficient (k_{scav}, s^{-1}) (Fan et al. 2012):

$$k_{scav} = \frac{F_{scav,1}P_{rain} + F_{scav,2}(1 - f_{berg})P_{snow} + F_{scav,3}f_{berg}P_{snow}}{Q_{liq} + Q_{ice}}, \quad (1)$$

where P_{rain} and P_{snow} are the 3-dimensional rain and snow rates (kg m^{-3} s^{-1}), respectively, and Q_{liq} and Q_{ice} the liquid and ice cloud water contents (kg m^{-3}), respectively. $F_{scav,i}$ is the scavenging efficiency (i.e. the fraction of BC that is incorporated into cloud droplets or ice crystals and removed by precipitation) for precipitation type i (i =1, 2, 3). f_{berg} is the fraction of snow produced by the Bergeron process. In this study, $F_{scav,1}$ and $F_{scav,2}$ are set to 0.2, and $F_{scav,3}$ is set to 0.01 to account for the less efficient removal of aerosols by snow produced by the Bergeron process than by rain and snow produced by riming and homogeneous freezing. Both hydrophobic and hydrophilic BC can be removed by below-cloud scavenging and dry deposition. The dry deposition velocity is calculated using the empirical resistance-in-series method with a surface-dependent

collection efficiency (Gallagher 2002), resulting in a much smaller dry deposition velocity over snow and ice than over land surfaces (soils and canopy).

3. Simulated and observed seasonal cycle of Arctic BC

Simulating Arctic BC, especially its seasonal cycle, remains a challenge for the current generation of models. Many models underestimate Arctic BC concentrations in winter by more than an order of magnitude and thus fail to reproduce the observed seasonal variations (Shindell et al. 2008). Figure 1 shows the AM3 simulated and observed monthly mean BC surface concentrations at Alert, Barrow, and Zeppelin (Eleftheriadis et al. 2009; Sharma 2004; Sharma et al. 2006). Measured BC exhibits similar seasonal variations at all three stations. Its concentrations peak in winter or early spring, followed by a rather precipitous decrease in April and May. The lowest concentrations occur from June to October. On average, BC concentrations in winter (DJF) are higher than in summer (JJA) by a factor of 3-4. The model is able to capture the seasonal cycle, but appears to underestimate BC at Alert and Barrow by a factor of 2-3 throughout the year. This discrepancy may result from model deficiencies, including uncertainties in BC emissions and deposition, or from observational errors, as some of the measurements are indirect and may be subject to rather large biases (Bond et al. 2013).

Figure 1 also compares the simulated BC vertical profiles at high latitudes (66°-85°N) with the aircraft measurements made during the HIAPER Pole-to-Pole Observations (HIPPO) campaigns (Schwarz et al. 2013; Wofsy 2011). The seasonal variations are evident in the data. In January, high concentrations of BC are confined within the boundary layer (HIPPO1). During early spring, there are enhancements of BC at higher altitudes (HIPPO3). BC concentrations at all altitudes start to decrease in June, and remain low throughout summer (HIPPO4 and HIPPO5). Despite overes-

timates in the free troposphere for some flights, the model generally performs well in simulating BC vertical profiles during all seasons.

Based on the above comparisons, we conclude that the model is capable of simulating the seasonal cycle of Arctic BC, and thus can be used to study its underlying mechanisms. This improvement in AM3 simulated Arctic BC is attributed to the modified BC-related processes (aging, wet removal and dry deposition) in the model, and Liu et al. (2011) discussed the sensitivity of BC simulation to each process in detail. Since observations show similar seasonality of Arctic BC at the surface and in the free troposphere, we will focus on the BC column burden averaged over the Arctic for the rest of the paper. This allows us to take full advantage of the model and generalize the results to the entire Arctic.

4. Controlling factors of Arctic BC

We employ a box model of the Arctic region to quantify the key factors controlling Arctic BC concentrations. Given the relatively small emissions from local sources, the prevailing balance is between the meridional BC transport into the Arctic and local deposition. One can write the rate of change in the average BC column burden (C, kg m^{-2}) as:

$$\frac{dC}{dt} = \frac{F}{S} - W - D, \tag{2}$$

where F is the total meridional flux into the Arctic (kg s^{-1}), S the Arctic surface area (m^2), and W and D the average wet and dry deposition rates (kg m^{-2} s^{-1}), respectively. Since the dry deposition of BC and the below-cloud scavenging of BCpo are small (less than 10% of the total BC deposition in the model simulation) and can be neglected, Eq. (2) can be simplified as:

$$\frac{dC}{dt} = \frac{F}{S} - W_{pi}, \tag{3}$$

where W_{pi} is the average BCpi wet deposition rate (kg m^{-2} s^{-1}). W_{pi} can be written as $r \cdot w \cdot C$, where r represents the dimensionless hydrophilic fraction of BC (C_{pi}/C, C_{pi} being the average BCpi column burden) and w represents the wet deposition efficiency of BCpi (W_{pi}/C_{pi}, s^{-1}), which can be thought of as the BC concentration-weighted in-cloud scavenging rate coefficient (k_{scav}) defined in Eq. (1), and is different from the wet scavenging efficiency ($F_{scav,i}$). As the AM3 simulated residence time of Arctic BC ranges from 6-20 days depending on the season (not shown), we assume steady state on the monthly time scale and arrive at an expression for C:

$$C = \frac{F}{S \cdot r \cdot w}. \tag{4}$$

An inspection of Eq. (4) suggests that elevated BC concentrations could result from stronger transport from mid-latitude source regions and/or weaker wet removal. General circulation patterns are important for determining long-rage transport fluxes. Wet removal is reduced when a smaller fraction of BC is hydrophilic or the wet deposition efficiency of BCpi is lower. The aging process exerts a strong control over the hydrophilic fraction. The wet deposition efficiency is affected mainly by the phase of precipitation because in-cloud scavenging efficiency differs among liquid, ice and mixed-phase clouds.

We apply the box model to quantify the roles of the three main variables, namely the meridional BC flux (F), BC hydrophilic fraction (r) and BCpi wet deposition efficiency (w), in controlling the seasonality of Arctic BC. The monthly mean values of F, r and w averaged over the Arctic (defined as poleward of 66°N) are computed from our AM3 model simulation. Figure 2a compares the monthly mean BC column burdens calculated using the box model with AM3 simulations. The good agreement validates the assumptions made in deriving Eq. (4). The box model captures the seasonal cycle, suggesting that one can rationalize the seasonality of Arctic BC by examining the three variables defined above.

5. Meridional transport

Like other anthropogenic aerosol species, BC is emitted mainly at the mid-latitude industrial regions and carried into the Arctic by atmospheric transport. Isentropic airflow facilitates high-level transport from warm and humid (high equivalent potential temperature, θ_e) areas such as North America and East Asia, and low-level transport from comparatively low θ_e areas such as Europe (Stohl 2006). Cross-isentropic transport due to diabatic heating or cooling also plays an important role (Klonecki et al. 2003). The total meridional BC flux (F) can be decomposed into contributions from the mean meridional circulation (MMC), stationary eddies, and transient eddies:

$$\{\overline{vc}\} = \underbrace{\{[\overline{v}][\overline{c}]\}}_{MMC} + \underbrace{\{\overline{v}^*\overline{c}^*\}}_{stationary\ eddies} + \underbrace{\{\overline{v'c'}\}}_{transient\ eddies}, \tag{5}$$

where v is the meridional wind velocity (m s^{-1}), and c the BC mass mixing ratio (kg kg^{-1}). Overbars denote monthly means, square brackets zonal means, asterisks deviations from zonal means, primes deviations from monthly means, and curly brackets zonal and vertical integrals (from the surface to $\sim$100 hPa). Figure 2b shows the annual cycle of the total monthly mean meridional BC flux into the Arctic (at 66°N) and its three components. Generally, the total BC flux does not show much variation with time. The average flux is only $\sim$20% higher in DJF than in JJA, far from sufficient to account for the column burden difference between the two seasons (Figure 2a). The contribution of the mean meridional circulation is very small. The transport is realized almost entirely by the eddy components. The flux by stationary eddies is comparable to that by transient eddies in DJF, while the latter dominates in JJA.

Although the vertically integrated BC flux changes little throughout the year, its vertical structure does vary with the season (Figure 3). The flux in DJF is characterized by two peaks (one in the boundary layer, and the other at about 500 hPa), which are of different origins. In winter the polar

dome (surface of constant potential temperatures) extends to about 40°N, allowing the low-level transport of BC from Europe (Stohl 2006). The diabatic cooling occurring when relatively warm air travels over a cold surface (i.e. strong inversion) keeps European BC in the boundary layer. The flux at about 500 hPa is more likely to be a result of transport from lower-latitude regions such as East Asia and North America. In JJA when BC from all regions experiences diabatic heating and wet removal caused by precipitation, the flux has only one notable peak at about 800 hPa originating from anthropogenic emissions in Europe and boreal forest fires over Eurasia. BC from North America and East Asia is more likely to be transported diabatically to higher altitudes, and diluted and rained out along the path to the Arctic (Klonecki et al. 2003).

We further explore the meridional BC flux in frequency space by applying a time filter. Since the mean meridional flux is negligible, $\{\overline{v_n c_n}\}$ approximates BC transport carried out by eddies with time scales greater than $2n$ days (Hall et al. 1994). Note that the subscript n denotes means of consecutive non-overlapping n-day periods. Figure 4 shows the time-filtered BC flux into the Arctic as a fraction of the total flux. The relative contributions from eddies of different frequencies to the total BC transport are different in the two seasons. In DJF, about 90% of the BC flux is realized by eddies with time scales longer than 10 days. Slightly more than 40% of the BC flux arises from eddies that persist longer than 60 days. In contrast, eddies with time scales longer than 10 days account for less than 50% of the JJA flux, and eddies that persist longer than 60 days have very little contribution to the total flux. Thus, while synoptic eddies dominate in JJA, low frequency eddies contribute substantially to the total transport in DJF.

The prominence of transient eddies in all seasons suggests that the long-range transport of Arctic haze can be represented, to first order, as turbulent diffusion of mid-latitude sources, despite the complexities at the process level (Shaw 1981). The idea of simplifying eddy transport as turbulent diffusion is widely used in understanding the atmospheric transport of heat and potential vorticity

(Held 1999). Here we apply it to study tracer transport. For a local down-gradient diffusion process, the vertically integrated meridional transient eddy BC flux can be assumed to be proportional to the meridional gradient of the BC column burden:

$$\{\overline{v'c'}\} = -D\frac{\partial}{\partial y}\{\overline{c}\}, \tag{6}$$

where D is the turbulent diffusivity. It is clear from Figure 5 that there is a strong negative correlation ($r = -0.75$) between the transient eddy flux and meridional gradient averaged at a number of latitudes between 40°-66°N. The magnitude of the slope of the best linear fit with zero intercept (2.24×10^6 m^2 s^{-1}) represents the eddy diffusivity, which is within the range of the estimated values in previous studies (e.g., Bolin and Keeling 1963; Newell et al. 1969; Held 1999). Note that this diffusivity does not change substantially with the season.

6. Hydrophilic fraction

Figure 6a shows the monthly mean hydrophilic fraction (r) of Arctic BC, which has a pronounced seasonal cycle that can be attributed to the parameterized aging mechanisms. The hydrophilic fraction in DJF is only ∼40%, while almost all BC is hydrophilic in JJA. The hydrophilic fraction of Arctic BC is very close to that of the meridional BC flux into the Arctic (Figure 6a), indicating that the annual cycle is shaped mainly by the aging process along the long-range transport path rather than locally in the Arctic. Figure 6b shows the monthly mean e-folding aging time of BC (the inverse of the aging rate coefficient, computed as the average BCpo concentration divided by the average conversion rate from BCpo to BCpi) at 40°-66°N and over the Arctic. During the transport from mid-latitudes to the Arctic, the average aging time is much longer in DJF (∼10 days) than in JJA (∼1 day), resulting in a substantially lower hydrophilic fraction in winter. In

the Arctic, the seasonal variations of BC aging time are even greater, which further amplifies the seasonal cycle of the hydrophilic fraction.

In the model the BC aging is assumed to result primarily from the condensation of H_2SO_4 onto BC aerosol surface, a common process that has been examined extensively in observational and experimental studies. H_2SO_4 is produced from the gas-phase oxidation of SO_2 by the OH radical and is rapidly converted to aerosol phase via nucleation or condensation onto existing particles. The aging rate is thus assumed to be proportional to OH concentrations. As a result of enhanced solar radiation and specific humidity, OH concentrations are much higher in JJA than in DJF, resulting in more rapid aging by condensation in summer. The aging can also occur through other processes (e.g. coagulation), which are believed to be slower and less important than condensation during long-range transport (Oshima et al. 2009). Therefore they are assumed to have a fixed e-folding time of 20 days, which is longer than that for the aging via condensation, and thus do not contribute to the seasonal cycle of the hydrophilic fraction.

The change in the hydrophilic fraction also helps explain the change in Arctic BC during spring and fall. From October to November, there is a sharp decrease in the hydrophilic fraction, resulting in a rapid buildup of BC. Similarly, from March to April, the increase in the hydrophilic fraction contributes to the decline in BC concentrations. The hydrophilic fraction, however, is fairly constant from April to September, in contrast with the continuous decrease in BC starting from April. The wet deposition efficiency plays an important role in driving BC changes during this time period, as discussed in the next section.

7. BCpi wet deposition efficiency

Figure 6c shows the monthly mean wet deposition efficiency of BCpi (w) in the Arctic. The wet deposition efficiency in JJA is $\sim$20% higher than in DJF, contributing to the lower BC in

JJA than in DJF. The magnitude of its seasonal cycle, however, is much weaker than that of the hydrophilic fraction (r) (Figure 6a). Yet, the wet deposition efficiency increases continuously by a factor of 2 from May to August, driving the transition from moderate BC burdens in late spring to exceedingly low burdens in summer.

The wet deposition efficiency is largely controlled by the in-cloud scavenging rate coefficient [k_{scav} in Eq. (1)]. To better understand the factors determining k_{scav}, we analyze the conversion rate coefficients of cloud condensate to rain (k_{rain}) and snow (k_{snow}) through which in-cloud scavenging occurs, which are defined as:

$$k_{rain} = \frac{P_{rain}}{Q_{liq} + Q_{ice}},\ k_{snow} = \frac{P_{snow}}{Q_{liq} + Q_{ice}}. \tag{7}$$

According to Eq. (1), k_{scav} and thus the wet deposition efficiency is determined by k_{rain} rather than k_{snow} in areas such as the Arctic where most snow is produced by the Bergeron process (Fan et al. 2012), since the scavenging efficiency for rain is much larger than for snow produced by Bergeron process. Figure 6d shows the annual cycle of AM3 simulated k_{rain} and k_{snow} in the Arctic. [P_{rain}, P_{snow}, Q_{liq} and Q_{ice} are first averaged over the Arctic and then k_{rain} and k_{snow} are calculated using Eq. (7)]. As the atmosphere becomes warmer and holds more water vapor from DJF to JJA, both rainfall (P_{rain}) and cloud water content ($Q_{liq} + Q_{ice}$) increase, and k_{rain} is higher in JJA than in DJF since rainfall increases more rapidly, consistent with the seasonal cycle of the wet deposition efficiency. From May to August, k_{rain} increases by a factor of 2, which helps explain the two-fold increase in the wet deposition efficiency. On the other hand, k_{snow} is much larger in DJF than in JJA because cold temperature favors snow formation, which is opposite to the seasonal variations in the wet deposition efficiency. Therefore one may expect that models without different removal efficiencies for liquid and mixed-phase clouds cannot reproduce the seasonal cycle of the wet deposition efficiency, and thus the seasonal cycle of Arctic BC concentrations.

8. Concluding remarks

It has long been recognized that aerosols from mid-latitude source regions undergo long-range transport and accumulate in the Arctic during late winter and early spring. Here we apply the GFDL AM3 model to analyze the key factors affecting the seasonal variations in Arctic BC. The model is able to reproduce the observed Arctic BC concentrations and seasonality, with 3-4 times higher values in DJF than in JJA. We find that the seasonal cycle of Arctic BC is caused mainly by the seasonality of wet deposition, with a secondary contribution from the long-range transport flux.

The transport of BC at mid- to high latitudes occurs mainly through stationary and transient eddies, rather than through the mean meridional circulation. Stationary eddies account for $\sim$40% of the total flux in DJF, while virtually all the transport is realized through transient eddies in JJA. The vertical distribution of meridional BC transport also varies seasonally. The vertical profile of the BC flux into the Arctic in DJF has two peaks (one in the boundary layer and the other in the mid-troposphere), while the BC flux in JJA is concentrated in the lower troposphere. The total meridional BC flux into the Arctic, however, changes little throughout the year despite the shift in large-scale circulation.

The wet removal depends on both BC hydrophilic fraction and BCpi wet deposition efficiency. The hydrophilic fraction is smaller in DJF than in JJA due to the slower BC aging along the long-range transport path to the Arctic during winter. This difference in the hydrophilic fraction plays a dominant role in the large difference in BC concentrations between DJF and JJA. The wet deposition efficiency is lower in DJF mainly because snow produced in mixed-phase clouds is less efficient in removing BC than rain. The decrease in BC concentrations from late spring to summer

is due to a gradual but steady increase in the wet deposition efficiency, while the return of BC in late autumn is mainly caused by a sharp decrease in the hydrophilic fraction.

Our results are consistent with the observational analysis of Garrett et al. (2011), which argued that some combination of dry deposition and wet scavenging drives the seasonal cycle of aerosols at low altitudes in the North American Arctic. Here we show that the dominance of wet deposition in determining BC seasonal cycle applies to the entire Arctic. We further explain the seasonality of wet deposition in terms of aging and cloud microphysical processes. While being influenced by complicated physical and chemical factors, these processes are parameterized in the model in a relatively simple way. Measurements of Arctic BC mixing state at different times are required for verifying the assumed OH dependence of the aging rate. Measurements of BC wet deposition and concentrations in rain and snow will be particularly useful for constraining the rain and snow scavenging efficiencies. It should also be noted that besides transport and wet deposition, large uncertainties remain in BC emission inventories, which have not been discussed in this paper. High-latitude BC emissions from gas flaring and residential combustion, which are underestimated or completely missing in most current inventories, have a large contribution to Arctic BC concentrations and are potentially crucial for affecting its seasonality (Stohl et al. 2013). However, as most of these BC emissions remain close to the surface, their contributions to BC in the mid- and upper troposphere in the Arctic are small (Stohl et al. 2013) and will not affect our conclusions, which are based on the BC column burden. Although the analysis in this paper focuses on BC, the findings should be generally applicable to other components of Arctic haze. For example, sulfate has a similar seasonal cycle, but with peak concentrations in spring as opposed to winter (as is the case for BC) (Shindell et al. 2008). The difference in the scavenging efficiencies by rain and snow probably dominates the seasonal variations in sulfate. Reducing wet deposition by snow has been found to improve model's ability to reproduce the observed sulfate concentrations over the United

States (Paulot et al. 2016) and in the Arctic (Browse et al. 2012). The shift in the peak may be due to the absence of an aging process since all sulfate is hydrophilic and the seasonal cycle of sulfate production by SO_2 oxidation.

The results discussed here may have implications for understanding the variability and trend in Arctic aerosols and their climate impacts. Since large-scale circulation influences the key processes of long-range transport and the spatial pattern of precipitation, natural climate variability at annual to decadal timescales may play an important role in determining changes in aerosol concentrations in the Arctic (Christoudias et al. 2012; Eckhardt et al. 2003). It would be interesting to apply our analysis to study the effect of climate variability on the characteristics of atmospheric transport and wet deposition. As climate warms, precipitation at high latitudes is expected to increase, but the fraction of snow may decrease (Barnett et al. 2005; Singarayer et al. 2006). These changes tend to enhance the wet scavenging of aerosols and result in a cleaner Arctic atmosphere. The aging process, which is affected by atmospheric composition, may also vary over time. SO_2 emissions at mid-latitudes have generally declined in recent decades (Streets et al. 2006) and are projected to decrease even more in the future (Levy et al. 2008). This long-term trend in SO_2 emissions will result in a decrease in sulfate concentrations but an increase in BC concentrations in the Arctic due to a slower aging process by condensation of H_2SO_4 and thus weaker wet removal. Therefore it is important to consider the changes in aerosol sources and sinks when using models to examine how aerosols may alter Arctic climate under future emission scenarios.

Acknowledgments. Songmiao Fan and Fabien Paulot provided helpful reviews of an earlier draft. We acknowledge the Science & Technology Branch at Environment Canada, the Global Monitoring Division at NOAA Earth System Research Laboratory, and Norwegian Institute for Atmospheric Research for providing measurement data. The observations at

Alert, Barrow, and Zeppelin are available through the Canadian Aerosol Baseline Measurement (CABM) Program Datasets (http://www.ec.gc.ca/donneesnatchem-natchemdata/default.asp?lang=En&n=22F5B2D4-1), the ESRL/GMD ftp site (/ftp.cmdl.noaa.gov/aerosol/brw/archive/), and World Data Center for Aerosol (EBAS) (http://ebas.nilu.no). The HIPPO data (Wofsy et al. 2012) are available at the CDIAC HIPPO data archive (http://hippo.ornl.gov/10secdownload/). Model simulations are archived at GFDL and are available from the authors upon request.

References

Barnett, T. P., J. C. Adam, and D. P. Lettenmaier, 2005: Potential impacts of a warming climate on water availability in snow-dominated regions. *Nature*, **438 (7066)**, 303–309, doi:10.1038/nature04141.

Barrie, L. A., 1986: Arctic air pollution: An overview of current knowledge. *Atmospheric Environment (1967)*, **20 (4)**, 643–663, doi:10.1016/0004-6981(86)90180-0.

Bindoff, N., and Coauthors, 2013: Detection and Attribution of Climate Change: from Global to Regional. *Climate Change 2013 - The Physical Science Basis*, Intergovernmental Panel on Climate Change, Ed., Cambridge University Press, Cambridge, 867–952, doi:10.1017/CBO9781107415324.022.

Bolin, B., and C. D. Keeling, 1963: Large-scale atmospheric mixing as deduced from the seasonal and meridional variations of carbon dioxide. *J. Geophys. Res.*, **68 (13)**, 3899–3920, doi:10.1029/JZ068i013p03899.

Bond, T. C., and Coauthors, 2013: Bounding the role of black carbon in the climate system: A scientific assessment. *J. Geophys. Res.*, **118 (11)**, 5380–5552, doi:10.1002/jgrd.50171.

Browse, J., K. S. Carslaw, S. R. Arnold, K. Pringle, and O. Boucher, 2012: The scavenging processes controlling the seasonal cycle in Arctic sulphate and black carbon aerosol. *Atmos. Chem. Phys.*, **12 (15)**, 6775–6798, doi:10.5194/acp-12-6775-2012.

Christoudias, T., A. Pozzer, and J. Lelieveld, 2012: Influence of the North Atlantic Oscillation on air pollution transport. *Atmos. Chem. Phys.*, **12 (2)**, 869–877, doi:10.5194/acp-12-869-2012.

Cozic, J., S. Mertes, B. Verheggen, D. J. Cziczo, S. J. Gallavardin, S. Walter, U. Baltensperger, and E. Weingartner, 2008: Black carbon enrichment in atmospheric ice particle residuals observed in lower tropospheric mixed phase clouds. *J. Geophys. Res.*, **113 (D15)**, D15 209, doi:10.1029/2007JD009266.

Donner, L. J., and Coauthors, 2011: The Dynamical Core, Physical Parameterizations, and Basic Simulation Characteristics of the Atmospheric Component AM3 of the GFDL Global Coupled Model CM3. *J. Climate*, **24 (13)**, 3484–3519, doi:10.1175/2011JCLI3955.1.

Eckhardt, S., and Coauthors, 2003: The North Atlantic Oscillation controls air pollution transport to the Arctic. *Atmos. Chem. Phys.*, **3 (5)**, 1769–1778, doi:10.5194/acp-3-1769-2003.

Eleftheriadis, K., S. Vratolis, and S. Nyeki, 2009: Aerosol black carbon in the European Arctic: Measurements at Zeppelin station, Ny-Ålesund, Svalbard from 1998-2007. *Geophys. Res. Lett.*, **36 (2)**, doi:10.1029/2008GL035741.

Fan, S.-M., and Coauthors, 2012: Inferring ice formation processes from global-scale black carbon profiles observed in the remote atmosphere and model simulations. *J. Geophys. Res.*, **117 (D23)**, D23 205, doi:10.1029/2012JD018126.

Friedman, B., G. Kulkarni, J. Beránek, A. Zelenyuk, J. A. Thornton, and D. J. Cziczo, 2011: Ice nucleation and droplet formation by bare and coated soot particles. *J. Geophys. Res.*, **116 (D17)**, D17 203, doi:10.1029/2011JD015999.

Gallagher, M. W., 2002: Measurements and parameterizations of small aerosol deposition velocities to grassland, arable crops, and forest: Influence of surface roughness length on deposition. *J. Geophys. Res.*, **107 (D12)**, 4154, doi:10.1029/2001JD000817.

Garrett, T. J., S. Brattström, S. Sharma, D. E. J. Worthy, and P. Novelli, 2011: The role of scavenging in the seasonal transport of black carbon and sulfate to the Arctic. *Geophys. Res. Lett.*, **38 (16)**, doi:10.1029/2011GL048221.

Hall, N. M. J., B. J. Hoskins, P. J. Valdes, and C. A. Senior, 1994: Storm tracks in a high-resolution GCM with doubled carbon dioxide. *Quart. J. Roy. Meteor. Soc.*, **120 (519)**, 1209–1230, doi:10.1002/qj.49712051905.

Held, I. M., 1999: The macroturbulence of the troposphere. *Tellus A*, **51 (1 SPEC. ISS.)**, 59–70, doi:10.3402/tellusa.v51i1.12306.

Iversen, T., and E. Joranger, 1985: Arctic air pollution and large scale atmospheric flows. *Atmospheric Environment (1967)*, **19 (12)**, 2099–2108, doi:10.1016/0004-6981(85)90117-9.

Janssens-Maenhout, G., and Coauthors, 2015: HTAP_v2.2: a mosaic of regional and global emission grid maps for 2008 and 2010 to study hemispheric transport of air pollution. *Atmos. Chem. Phys.*, **15 (19)**, 11 411–11 432, doi:10.5194/acp-15-11411-2015.

Klonecki, A., P. Hess, L. Emmons, L. Smith, J. Orlando, and D. Blake, 2003: Seasonal changes in the transport of pollutants into the Arctic troposphere-model study. *J. Geophys. Res.*, **108 (D4)**, 8367, doi:10.1029/2002JD002199.

Law, K. S., and A. Stohl, 2007: Arctic air pollution: origins and impacts. *Science*, **315 (5818)**, 1537–40, doi:10.1126/science.1137695.

Levy, H., M. D. Schwarzkopf, L. Horowitz, V. Ramaswamy, and K. L. Findell, 2008: Strong sensitivity of late 21st century climate to projected changes in short-lived air pollutants. *J. Geophys. Res.*, **113 (D6)**, D06 102, doi:10.1029/2007JD009176.

Lin, M., and Coauthors, 2012: Transport of Asian ozone pollution into surface air over the western United States in spring. *J. Geophys. Res.*, **117 (D21)**, doi:10.1029/2011JD016961.

Liu, J., S. Fan, L. W. Horowitz, and H. Levy, 2011: Evaluation of factors controlling long-range transport of black carbon to the Arctic. *J. Geophys. Res.*, **116 (D4)**, D04 307, doi:10.1029/2010JD015145.

Mitchell, J. M., 1957: Visual range in the polar regions with particular reference to the Alaskan Arctic. *J. Atmos. Terr. Phys. Spec. Suppl*, 195–211.

Newell, R. E., D. G. Vincent, and J. W. Kidson, 1969: Interhemispheric mass exchange from meteorological and trace substance observations. *Tellus A*, doi:10.3402/tellusa.v21i5.10114.

Oshima, N., M. Koike, Y. Zhang, and Y. Kondo, 2009: Aging of black carbon in outflow from anthropogenic sources using a mixing state resolved model: 2. Aerosol optical properties and cloud condensation nuclei activities. *J. Geophys. Res.*, **114 (D18)**, D18 202, doi:10.1029/2008JD011681.

Paulot, F., and Coauthors, 2016: Sensitivity of nitrate aerosols to ammonia emissions and to nitrate chemistry: implications for present and future nitrate optical depth. *Atmos. Chem. Phys.*, **16 (3)**, 1459–1477, doi:10.5194/acp-16-1459-2016.

Petters, M. D., A. J. Prenni, S. M. Kreidenweis, P. J. DeMott, A. Matsunaga, Y. B. Lim, and P. J. Ziemann, 2006: Chemical aging and the hydrophobic-to-hydrophilic conversion of carbonaceous aerosol. *Geophys. Res. Lett.*, **33 (24)**, L24 806, doi:10.1029/2006GL027249.

Quinn, P. K., G. Shaw, E. Andrews, E. G. Dutton, T. Ruoho-Airola, and S. L. Gong, 2007: Arctic haze: current trends and knowledge gaps. *Tellus B*, **59 (1)**, 99–114, doi:10.1111/j.1600-0889.2006.00238.x.

Scheuer, E., 2003: Seasonal distributions of fine aerosol sulfate in the North American Arctic basin during TOPSE. *J. Geophys. Res.*, **108 (D4)**, 8370, doi:10.1029/2001JD001364.

Schwarz, J. P., and Coauthors, 2013: Global-scale seasonally resolved black carbon vertical profiles over the Pacific. *Geophys. Res. Lett.*, **40 (20)**, 5542–5547, doi:10.1002/2013GL057775.

Sharma, S., 2004: Long-term trends of the black carbon concentrations in the Canadian Arctic. *J. Geophys. Res.*, **109 (D15)**, D15 203, doi:10.1029/2003JD004331.

Sharma, S., E. Andrews, L. a. Barrie, J. a. Ogren, and D. Lavoué, 2006: Variations and sources of the equivalent black carbon in the high Arctic revealed by long-term observations at Alert and Barrow: 19892003. *J. Geophys. Res.*, **111 (D14)**, D14 208, doi:10.1029/2005JD006581.

Shaw, G., 1981: Eddy diffusion transport of Arctic pollution from the mid-latitudes: A preliminary model. *Atmospheric Environment (1967)*, **15 (8)**, 1483–1490, doi:10.1016/0004-6981(81)90356-5.

Shindell, D., and G. Faluvegi, 2009: Climate response to regional radiative forcing during the twentieth century. *Nat. Geosci.*, **2 (4)**, 294–300, doi:10.1038/ngeo473.

Shindell, D. T., and Coauthors, 2008: A multi-model assessment of pollution transport to the Arctic. *Atmos. Chem. Phys.*, **8 (17)**, 5353–5372, doi:10.5194/acp-8-5353-2008.

Singarayer, J. S., J. L. Bamber, and P. J. Valdes, 2006: Twenty-First-Century Climate Impacts from a Declining Arctic Sea Ice Cover. *J. Climate*, **19 (7)**, 1109–1125, doi:10.1175/JCLI3649.1.

Stohl, A., 2006: Characteristics of atmospheric transport into the Arctic troposphere. *J. Geophys. Res.*, **111 (D11)**, D11 306, doi:10.1029/2005JD006888.

Stohl, A., Z. Klimont, S. Eckhardt, K. Kupiainen, V. P. Shevchenko, V. M. Kopeikin, and a. N. Novigatsky, 2013: Black carbon in the Arctic: the underestimated role of gas flaring and residential combustion emissions. *Atmos. Chem. Phys.*, **13 (17)**, 8833–8855, doi:10.5194/acp-13-8833-2013.

Streets, D. G., Y. Wu, and M. Chin, 2006: Two-decadal aerosol trends as a likely explanation of the global dimming/brightening transition. *Geophys. Res. Lett.*, **33 (15)**, L15 806, doi:10.1029/2006GL026471.

Wiedinmyer, C., S. K. Akagi, R. J. Yokelson, L. K. Emmons, J. a. Al-Saadi, J. J. Orlando, and a. J. Soja, 2011: The Fire INventory from NCAR (FINN): a high resolution global model to estimate the emissions from open burning. *Geosci. Model Dev.*, **4 (3)**, 625–641, doi:10.5194/gmd-4-625-2011.

Wofsy, S. C., 2011: HIAPER Pole-to-Pole Observations (HIPPO): fine-grained, global-scale measurements of climatically important atmospheric gases and aerosols. *Philos. Trans. R. Soc., A*, **369 (1943)**, 2073–2086, doi:10.1098/rsta.2010.0313.

Wofsy, S. C., and Coauthors, 2012: HIPPO Merged 10-second Meteorology, Atmospheric Chemistry, Aerosol Data. $(R\_20121129)$. Carbon Dioxide Information Analysis Center, Oak Ridge National Laboratory, Oak Ridge, Tennessee, U.S.A. $http://dx.doi.org/10.3334/CDIAC/hippo\_010$ $(Release 20121129)$.

Zhang, R., A. F. Khalizov, J. Pagels, D. Zhang, H. Xue, and P. H. McMurry, 2008: Variability in morphology, hygroscopicity, and optical properties of soot aerosols during atmospheric processing. *Proc. Natl. Acad. Sci. (USA)*, **105 (30)**, 10 291–10 296, doi:10.1073/pnas.0804860105.

LIST OF FIGURES

Fig. 1. (top) Model simulated and observed monthly mean surface BC at Alert (2008-2012), Barrow (2008-2013), and Zeppelin (2008-2013). Error bars denote one standard deviation from monthly means. (bottom) Model simulated and observed BC vertical profiles at high latitudes (66°-85°N) during HIPPO (HIPPO1: January 2009, HIPPO2: October-November 2009, HIPPO3: March-April 2010, HIPPO4: June-July 2011, HIPPO5: August-September 2011). Error bars associated with observational profiles represent one standard deviation of the HIPPO data. For the comparison, daily BC fields archived from the model are first sampled along the flight track and then averaged over 66°-85°N for each campaign. 26

Fig. 2. Monthly mean (a) Arctic BC column burdens simulated using AM3 (red) and derived from the box model (black), (b) AM3 simulated total meridional BC flux into the Arctic (solid) and contributions from the mean meridional circulation (dashed), stationary eddies (dash-dot), and transient eddies (dotted). Error bars denote one standard deviation from monthly means. 27

Fig. 3. Vertical profiles of meridional BC flux at 66°N. The solid and dashed lines represent DJF and JJA, respectively. 28

Fig. 4. Time-filtered meridional BC flux ($\{\overline{v_n c_n}\}$ defined in Section 5) as a fraction of total flux at 66°N. The solid and dashed lines represent DJF and JJA, respectively. 29

Fig. 5. Scatter plot of vertically integrated monthly mean meridional BC flux by transient eddies versus meridional gradients of BC column burden averaged over 40°-66°N. The linear regression line is also shown. Green and red dots represent DJF and JJA, respectively. 30

Fig. 6. Monthly mean AM3 simulated (a) hydrophilic fractions of Arctic BC (solid) and BC flux into the Arctic (dashed), (b) BC aging time averaged at 66°-90°N (solid) and 40°-66°N (dashed), (c) Arctic BCpi wet deposition efficiency, and (d) rate coefficients of conversion of cloud condensate to rain (solid) and snow (dashed) in the Arctic. Error bars denote one standard deviation from monthly means. 31

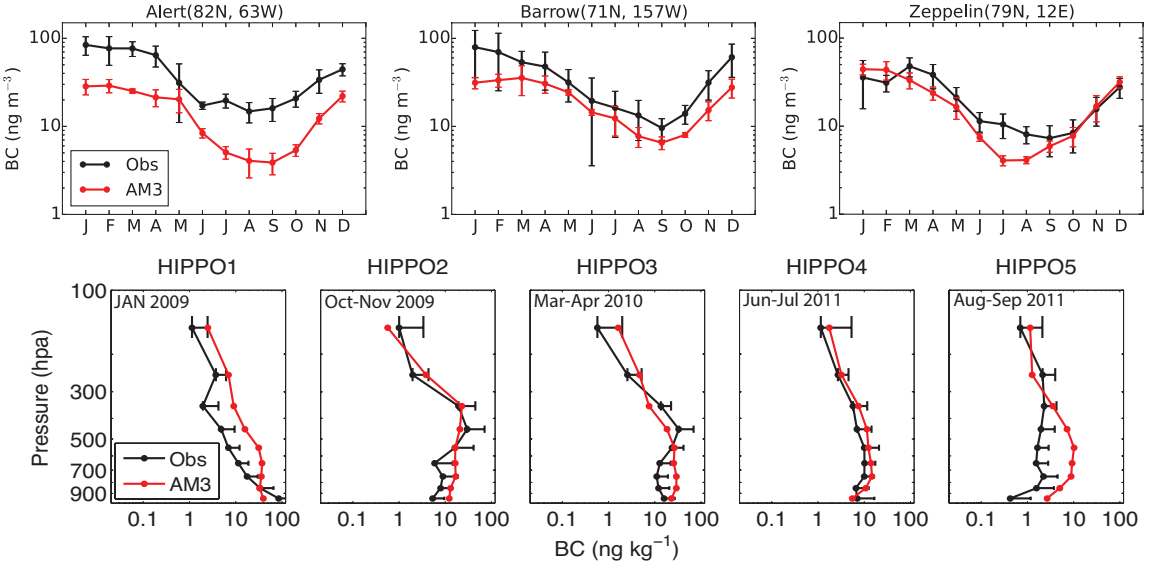

519 FIG. 1. (top) Model simulated and observed monthly mean surface BC at Alert (2008-2012), Barrow (2008-
520 2013), and Zeppelin (2008-2013). Error bars denote one standard deviation from monthly means. (bottom)
521 Model simulated and observed BC vertical profiles at high latitudes (66°-85°N) during HIPPO (HIPPO1: Jan-
522 uary 2009, HIPPO2: October-November 2009, HIPPO3: March-April 2010, HIPPO4: June-July 2011, HIPPO5:
523 August-September 2011). Error bars associated with observational profiles represent one standard deviation of
524 the HIPPO data. For the comparison, daily BC fields archived from the model are first sampled along the flight
525 track and then averaged over 66°-85°N for each campaign.

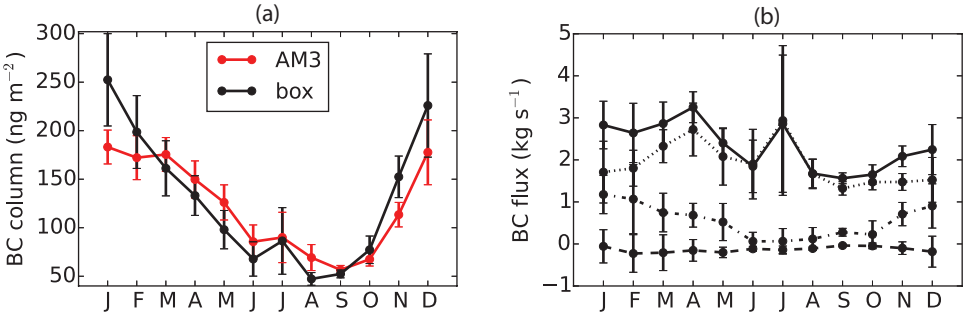

526 FIG. 2. Monthly mean (a) Arctic BC column burdens simulated using AM3 (red) and derived from the box
527 model (black), (b) AM3 simulated total meridional BC flux into the Arctic (solid) and contributions from the
528 mean meridional circulation (dashed), stationary eddies (dash-dot), and transient eddies (dotted). Error bars
529 denote one standard deviation from monthly means.

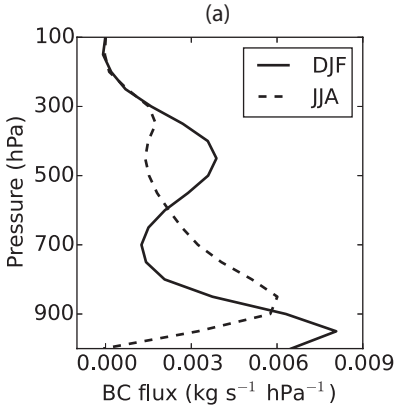

FIG. 3. Vertical profiles of meridional BC flux at 66°N. The solid and dashed lines represent DJF and JJA, respectively.

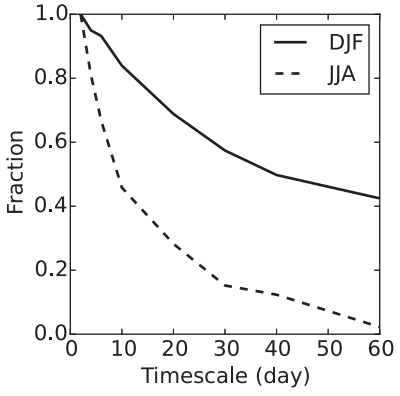

532 FIG. 4. Time-filtered meridional BC flux ($\{\overline{v_n c_n}\}$ defined in Section 5) as a fraction of total flux at 66°N. The
533 solid and dashed lines represent DJF and JJA, respectively.

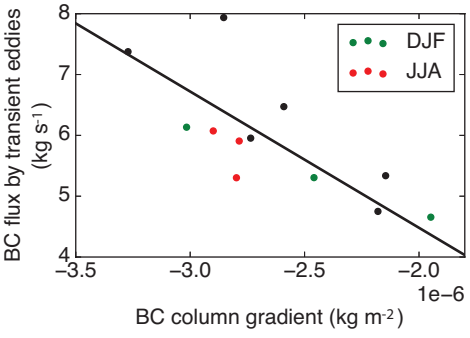

534 FIG. 5. Scatter plot of vertically integrated monthly mean meridional BC flux by transient eddies versus
535 meridional gradients of BC column burden averaged over 40°-66°N. The linear regression line is also shown.
536 Green and red dots represent DJF and JJA, respectively.

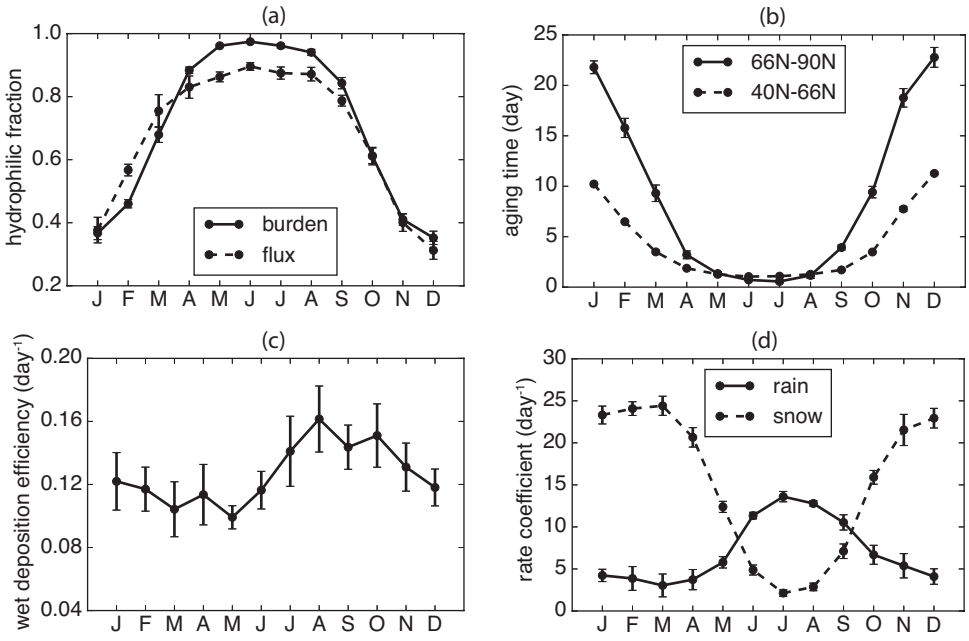

537 FIG. 6. Monthly mean AM3 simulated (a) hydrophilic fractions of Arctic BC (solid) and BC flux into the
538 Arctic (dashed), (b) BC aging time averaged at 66°-90°N (solid) and 40°-66°N (dashed), (c) Arctic BCpi wet de-
539 position efficiency, and (d) rate coefficients of conversion of cloud condensate to rain (solid) and snow (dashed)
540 in the Arctic. Error bars denote one standard deviation from monthly means.